HHS Public Access

Author manuscript

Phys Chem Chem Phys. Author manuscript; available in PMC 2015 December 14.

Published in final edited form as:

Phys Chem Chem Phys. 2014 December 14; 16(46): 25523–25530. doi:10.1039/c4cp04031g.

Effect of Metal Film Thickness on Tamm Plasmon-Coupled Emission

Yikai Chen[1], **Douguo Zhang**[1,*], **Liangfu Zhu**[1], **Qiang Fu**[1], **Ruxue Wang**[1], **Pei Wang**[1], **Hai Ming**[1], **Ramachandram Badugu**[2], and **Joseph R. Lakowicz**[2,*]

[1]Institute of Photonics, Department of Optics and Optical Engineering, University of Science and Technology of China, Hefei, Anhui, 230026, China

[2]Center for Fluorescence Spectroscopy, Department of Biochemistry and Molecular Biology, University of Maryland School of Medicine, Baltimore, MD 21201, USA.

Abstract

Tamm plasmons (TPs) are the result of trapping optical energy at the interface between a metal film and a one-dimensional photonic crystal. In contrast to surface plasmons, TPs display unique properties such as the ability of direct optical excitation without the aid of prisms, or gratings, being populated using both S- and P- polarized light, and importantly, they can be created with incident light normal to the surfaces. This latter property has recently been used to obtain Tamm plasmon-coupled emission (TPCE) which beams along a path directly perpendicular to the surface. In this paper the effects of metal film thickness on TPCE are investigated using back focal plane (BFP) imaging and spectral resolutions. The observed experimental results are in agreement with the numerical simulations. The present work provides the basic understanding to design the structures for TPCE, which in turn has potential applications in the fabrication of the active material for light emitting devices, fluorescence based-sensing using microarrays and imaging.

Keywords

Fluorescence; Tamm Plasmons; Tamm Plasmon-Coupled Emission; Metal film; Back Focal Plane imaging

1: Introduction

Controlling the emission from the active materials, such as dye molecules or semiconductor quantum dots, is an important area of research which has widespread applications in light emitting devices (LEDs), fluorescence-based sensing and imaging [1,2]. This interest is due to the realization that the fluorescence technology is reaching some natural limits when using classical far-field free-space optics. Current day fluorescence measurements rely upon the unperturbed free-space emission of fluorophores and subsequent manipulation of free-space light by external optical components. Due to the inherent omni-directional nature of the free-space emission, signal collection from the active materials is very low, less than a

*dgzhang@ustc.edu.cn, JLakowicz@som.umaryland.edu.

few percent of the total emission. To obtain new opportunities with the fluorescence technology we have been working on the near-field coupled fluorescence where we use the interaction of the probes with metallic particles or metal surfaces to increase the brightness of the probes and/or converting the omni-directional emission into directional emission [3–6]. The principles of this work rely on the localized surface plasmons (LSPs) or surface plasmons (SPs) which are present on or inside these metal nanostructures [7, 8]. The near-field effects of LSPs or SPs can accelerate the spontaneous emission rates of molecules and thus induce fluorescence enhancement [9]. The emitting direction from the fluorophores can also be controlled. We termed these phenomena as Metal-Enhanced Fluorescence (MEF) and Surface Plasmon-Coupled Emission (SPCE), respectively. In SPCE the fluorophores within a near-field distance of thin metal film can couple to the SPs and induce the directional emission [10–11]. The SPCE can be seen as an inverse process of the SPs' excitation through the Kretschmann configuration [12–13].

Directional emission can also be achieved using probes within near-field distances from the dielectric photonic crystals (PCs), where a periodic modulation of the dielectric function on a scale comparable to the wavelength of interest provides control of light propagation, including even confinement below the diffraction limit. It has been recently shown that Bloch surface waves (BSWs) on PCs can induce the Bloch surface wave-coupled emission (BSWCE) [14–22]. For SPCE and BSWCE, the emitting angle is always larger than the total internal reflection angle (TIRA), or critical angle of the glass-air interface. Another approach is to use optical antennas made of metal nanostructures to manipulate the fluorescence with emitting angle near normal to the surface (zero angle). Fabrication of this kind of optical antenna requires high-cost nanofabrication methods, which are currently not practical for large-area applications such as micro-plate sensing [23–29]. Also, it is difficult to uniquely position fluorophores at the active region of these structures. Tamm plasmon-coupled emission (TPCE) takes advantage of the small or near-zero in-plane wavenumber of Tamm plasmons (TPs) and shows directional emission close to the surface normal. In contrast to the SPs, TPs exist at the interface between the metal film and a dielectric Bragg reflector and can be populated with both S- and P-polarized light [30–40]. Because the wave-vector of the TPs is smaller than that of light in vacuum at the same frequency, it can be excited directly without the aid of prisms or gratings. The Tamm structures described in this report are simple to be fabricated over large areas using only deposition methods. The beaming near normal fluorescence emission has potential applications for the high throughput fluorescence sensing or detection [41–42]. Due to these unique merits, it is of great importance to understand the factors that affect the performance of the TPCE. In this paper, we focused on the effects of top metal film thickness on the performances of TPCE, which has not been reported before. Our results show that the intensity of the TPCE is sensitive to the thickness of the top metal film but the angular divergent remains mostly constant. The results shown herein demonstrate that Tamm structures are valuable for high sensitive fluorescence related technologies and high efficiency LEDs.

2: Samples preparation and numerical simulation

Figure 1 (a) shows the schematic of the Tamm structure, which consists of a one-dimensional photonic crystal (1DPC) [14–22] and a silver layer. In the absence of metal,

BSWs can be generated on top surface of this 1DPC [17]. The resonant wavelength and resonant angle of BSWs are strongly dependent on the structural parameters and sensitive to the surrounding medium, which enables applications in sensing and fluorescence emission (direction or spectral) modulation [43–48]. For the present paper this 1DPC was coated with silver films. The dielectric layers were fabricated with the plasma-enhanced chemical vapor deposition (PECVD) method. Alternate layers of SiO_2 (a low refractive index material) and Si_3N_4 (a high refractive index material) were deposited on a standard microscope cover glasses (0.17 mm thickness) with large area (24 mm by 50 mm). Prior to PECVD, the cover glasses were cleaned with piranha solution, washed with deionized water and finally dried with air stream. The conditions for SiO_2 deposition were 5% SiH_4/N_2 and NO_2 at 300°C with 400 SCCM overall gas flow. The deposition rate is 40 nm per min. Si_3N_4 layers were obtained while using 5% SiH_4/N_2 and NH_3 at 300°C with 400 standard cubic cm per minute (SCCM) overall gas flow. The thickness and refractive index (at 632 nm) of the single layer of SiO_2 or Si_3N_4 on silicon wafer were measured using an N- and K-spectral ellipsometer (model 1200). Further details on the 1DPC fabrication can be found in our previous paper [17]. The top SiO_2 layer has a thickness of 152 nm, the thicknesses of other SiO_2 and Si_3N_4 layers of the 1DPC were 126 and 78 nm, respectively. These structural parameters were obtained from numerical simulations. The numerical simulations are based on the transfer matrix method (TMM). These optimized parameters were selected to obtain the TPs as needed for our range of wavelengths. A PMMA film with thickness of approximately 49 nm was spin-coated on to the top SiO_2 layer. The active medium, Nile Blue (NB) molecules from Sigma-Aldrich, are doped in the PMMA film. Finally, the Ag film was evaporated onto the PMMA film. The thickness (t) of Ag film is varied from sample to sample. In our experiment, the t was selected as 0, 10, 20, 30, 55 nm and 100 nm. Figure 1(b) shows the atomic force microscopy (AFM) image of the 10 nm thick Ag film on the 1DPC (Figure 1(a)). The metal film was continuous at 10 nm and larger thicknesses. The surface structure heights are small compared to a typical silver island film [49].

The transfer matrix method (TMM) is used to calculate the angle-dependent reflectivity from the Tamm strucutrue with different Ag films thicknesses. The dimensions used for the simulations are the same as shown in Figure 1 (a). A plane wave illuminates the Tamm sample from the glass substrate with the angle θ. The normalized reflectivity is defined as R/I, where R represents the intensity of reflected light and I is the intensity of incident light. Figure 2 presents the calculated angle-dependent reflectivity of the Tamm structures with different thicknesses of Ag films. The veritical axis represents the thickness of the Ag film and the horizontal axis shows the incident angle (θ). The scale bar represents the normalized reflectivity. The polarization states of the incident light are transverse-magnetic or P-polarized (TM, Figure 2a) and transverse-electric or S-polarized (TE, Figure 2b). TM light is polarized along the z-axis and TE light is polarized along the x-axis (Figure 1). The wavelength of the incident light is 680 nm. The refractive indexes of the glass substrate, SiO_2, Si_3N_4, Ag, and PMMA at 680 nm wavelengths are 1.518, $1.46+10^{-5}i$, $2.14+10^{-5}i$, 0.14+4.44i, and $1.49+10^{-5}i$, respectively.

The decreases in the reflectivity correspond to excitation of the confined optical modes inside or on the Tamm structure, such as the SPs, TPs, and guided modes (GMs), representing that the energy of the incident light transfers into these confined modes [50].

These modes have different resonant angles and can be resolved from the electric field intensities (E^2) distribution at the corresponding resonant angles. The reflectance drops in Figure 2, depending on the field location in the structure, can be attributed to the SPs, TPs, or GMs. The image plot clearly indicates the effect of Ag film thickness on excitation of these modes. For example, when the light is TM polarized, the SPs (locally confined at the Ag-Air interface) can be excited only when the Ag film is in a certain thickness range (approximately, from 20 nm to 60 nm). In this range, the resonant angles of SPs near 42° decrease slightly with the increasing thickness of the Ag films. The surface plasmon resonant (SPR) dips (Figure 2a, the blue strip marked with “SPs”) on the reflection curves at fixed thickness of Ag film become narrow with the increasing Ag film thickness, which means lower propagation loss of the SPs (Ag-Air interface). The resonant angle of the SPs is around 42.9°, which is larger than the TIRA of Glass-Air interface (41.2°). These decreases in reflectivity are not presented with TE polarization, demonstrating that the TM bands are due to SPs.

In contrast to SPs, the TPs are accessible with incident light normal to the surface. The TPs cannot be sustained when the Ag film is too thin, for example, less than about 20 nm. When the Ag film is very thin (less than about 20 nm), and the incident angle is smaller than the TIRA, TPs do not exist on the structure. The reason for this phenomenon can be described as following: the TPs, sometimes called Tamm plasmon polaritons (TPPs), are a trapped electro-magnetic state that exists between a metal and a dielectric Bragg reflector where the electric-magnetic field is highly confined. The confinement in the dielectric multilayer structure is due to the photonic stop band of the Bragg reflector. To realize the photonic stop band, as many as 14 layers of the dielectric films were used. The electric-field confinement by the metal is achieved as a result of its negative dielectric constant [30]. But when the metal film is too thin, such as 20nm or less, the effective dielectric constant of the upper space (including metal film and air) will not be negative enough to confine the optical field. With the increase of Ag film thickness, the effective dielectric constant of the upper space will be dominated by the metal film and the Tamm mode can exist.

The dimensions of the structure were selected so that the resonant angle of TPs is near normal to the glass substrate (0°). The angular divergence of TPs becomes smaller and remains constant with additional increases of the Ag film thickness (larger than 60 nm), as illustrated in Figure 2. We note that the TPs remain even very thick Ag films. The other difference between the TPs and SPs is that the TPs can be excited by both the TM and TE polarized light (Figure 2a and b), while SPs can be populated only by the TM polarized illumination (Figure 2a). Apart from the TPs, GMs also appear in the case of TE polarized light (Figure 2b) illumination. The GMs are guided optical energy inside the 1DPC and similar as the guided waves loaded by the planar waveguides. The GMs exist for all thickness of the Ag films. The resonant angles of the two GMs are about 50.1° and 62.8°, respectively, which are larger than the TIRA, so the electric filed of the GMs above the Tamm samples is evanescent. When the incident light is TM polarized, cavity modes (CMs) with optical energy oscillating inside the 1DPC appear (triangle blue shape at the bottom of Figure 2 a). The resonant angle of the CMs is around 39° which is smaller than the TIRA of glass-air interface. Hence the optical field above the Tamm samples is propagating and there is light transmitted through the Tamm samples at these incident angles. The electric filed

distribution of CMs inside the Tamm samples is like an oscillating field between two mirrors with low reflectivity, so we call them as cavity modes [50]. The dips of the CMs on the reflectivity curves are due to both the absorption and transmission of the Tamm samples, whose width is larger than those of SPs, GMs. With the increase of Ag film thickness, the CMs disappear due to the large reflectivity of top thick Ag films.

Figure 2 clearly demonstrates the relation between Ag film thickness and confined optical modes existing in the Tamm structures and it also reveals the resonant angles of these modes are sensitive to the metal layer thickness. The resonant angles of SPs and GMs are all larger than the TIRA, so the emission angle of the fluorescence coupled with these modes will be larger. For example, considering the case with an Ag film above 20 nm thick. Without the aid of a prism, grating or small roughness, these modes cannot be excited and the corresponding coupled emissions (SPCE, BSWCE) cannot radiate into the free space, which is the +Z direction in Figure 1. On the other hand, the resonant angle of TPs is very small, almost near zero, and can be excited directly with free space light, so the TPCE will be near-normal to the planar substrate. We experimentally investigated the effects of metal film thickness on the TPs and TPCE from the reflection spectra, fluorescence spectra, and back focal plane (BFP) images, which will be compared with the above numerical simulations.

3: Experimental results and discussion

The Tamm structure reflectivity spectra for the normal incidence (Figure 1a) were measured with the reflection mode of a spectrometer from Ocean Optics, USA. The schematic of the experimental set-up for the reflectivity measurement is shown in Figure 3a. White light from a Halide lamp (Ocean Optics) is coupled into one end of a bifurcated optic fiber (R400-7-UV-VIS reflection probe); the other end of this fiber is coupled into the spectrometer (USB 4000). The white light illuminates the Tamm structures from the glass side, through the multi-layer dielectrics, and then reflects back into the spectrometer. The reflectivity spectrum from a thick Ag film (complete mirror) on a glass substrate is used as the reference. The measured reflectivity curves normal to the surface from the Tamm structures are shown in Figure 3(b). The selected thickness of the Ag films of the Tamm samples are 0, 10, 20, 30, 55 and 100 nm. For the bare 1DPC (that is with 0 nm thick Ag film), a high reflectivity band from 620 nm to 750 nm wavelength is noticed, which corresponds to the photonic band gap (PBG) of this 1DPC [51]. The high reflectivity band was still preserved when the thickness of Ag film is less than about 20 nm. When the thickness of Ag film increases to 30 nm, a shallow and broad dip appears at about 681 nm. With the increase of Ag film thickness to 55 nm and 100 nm the corresponding reflectivity dip becomes deep and narrow.

The appearance and change of the dips with Ag film thickness can be understood from the numerical simulation shown in Figure 2. When the Ag film is very thin, less than about 20 nm, and the incident angle is smaller than the TIRA, TPs cannot exist on the structure and the light is reflected to the PBG. The TPs become strong when the thickness of Ag film is increased to 30 nm, or to 55 nm and 100 nm. The incident light is transferred into the confined TPs, which results in the reflection minimum. This transfer is probably due to the evanescent of the incident light and the 1DPC. As shown in Figure 2, for both TE and TM

polarized incident light, the Tamm plasmon resonant angle (TPRA) of the Tamm structure at 680 nm wavelength is zero degrees. Experimentally, a dip at 681 nm wavelength appears on the normal reflection curve.

The fluorescence spectra from the Tamm structures with various thick Ag films were measured with the experimental set-up shown in Figure 4a. A low numerical aperture (N.A = 0.16) objective (4×) is used to weakly focus the 532 nm wavelength laser beam onto the Tamm samples from the glass substrate. Under excitation, the fluorescence from the Nile Blue (NB) molecules doped in the PMMA layer (Figure 1(a)) is collected by the same objective. A low N.A. objective is used so that only near normal emission is collected. Based on the N.A. of the objective, the collection angle range can be derived as from −9.2° to 9.2°. A control sample made of glass-NB doped PMMA −100 nm thick Ag (where the multi-layer 1DPC is removed from the Tamm structures as shown in Figure 1a) is fabricated. The fluorescence spectrum from the control sample is measured for comparison, which displays broad-band emission as shown in Figure 4(b). For NB on the 1DPC (no Ag film) the emission is strongly suppressed especially within the band from 620 nm to 750 nm wavelength. This phenomenon can be attributed to the band-gap of the 1DPC. The suppressed spectrum curve remains the same when the thickness of Ag film is 10 nm or 20 nm. When the thickness of the Ag film increases to 30 nm, an emission peak appears with center wavelength at 680 nm. With thicker Ag films, such as 55 nm and 100 nm, the emission peak at 680 nm becomes more intense than the peak intensity on the emission spectrum from the control sample. The spectra measured here show that the observed emission spectra from the NB are strongly modulated by the Tamm structures. This phenomenon can be explained through the normal reflection curves shown in Figure 3(b). The reflection spectra represents the energy conversion from far-field light to the confined optical modes (such as SPs, TPs, CMs, and GMs), while the emission spectra represents the energy conversion from near-field optical energy (such as excited optical emitters) to the far-field light via the confined optical modes, they are reverse processes. The dip on the reflection spectrum corresponds to the peak of the fluorescence spectrum, which are both near the 680 nm. The peaks or dips appear only when the Ag film is 30 nm or thicker, so we can assume that the strong emission peaks at 680 nm wavelength can be attributed to the emission coupling with the TPs. The strong peak at 680 nm may be the result of spectral redistribution from the broad emission to a narrow band. Additional experiments are required to address this properly.

The electric field of TPs is localized below the Ag film where the NB molecules in the PMMA film are located. Under excitation, the NB molecules will couple with the TPs thus enabling the TPCE. The TPs are very sensitive to the wavelength and only fluorescence at the resonant wavelength can couple efficiently with them, which results in the narrow peak at 680 nm wavelengths as shown in Figure 4(b). The modulated fluorescence spectra also demonstrate the intensity difference of TPCE in cases of different Ag film thickness.

The effect of Ag film thickness on the angular radiation patterns of the TPCE was investigated with BFP imaging. The experimental set-up for BFP imaging is similar to that shown in Figure 4 (a), except an objective lens with N.A as 1.42 (60 ×) is used, which corresponds to the angle (θ) range from −69° to +69°. Due to the large collection angle of

the objective, the fluorescence emission coupled with SPs, TPs, and GMs can be imaged. Further details of the BFP imaging set-up can be found in references [52–56]. A band-pass filter with center wavelength of 680 nm is placed before the detector sCMOS camera, so that only fluorescence at the Tamm plasmon resonant wavelength (TPRW) is imaged. A horizontal polarizer is included before the sCMOS to determine the polarization states of the coupled emissions. Figures 5(a – e) present the fluorescence BFP images from Tamm structures with Ag thicknesses of 10, 20, 30, 55 and 100 nm, respectively. The fluorescence BFP image of the control Ag mirror sample is also presented in Figure 5f.

Each point on the fluorescence BFP image corresponds to an emitting angle of the 680 nm wavelength fluorescence. The closer the point to the center of the BFP image, the smaller its emitting angle. The TP resonance angle of our structure is near zero, so that the TPCE will appear on the center of the BFP image. When the thickness of Ag film is 10 or 20 nm, there is no fluorescence at the center of the BFP images, which indicates the absence of TPCE. The two BFP images (Figure 5a and b) are consistent with the numerical simulation and experimental spectral reflectances discused above. When the thickness of Ag film increases to 30 nm, a weak disk appears on the center of Figure 5(c). With further increasing the thickness of Ag layer, the disk becomes much brigther and more concentrated as shown in Figures 5(d) and (e). This result indicates that the TPCE becomes stronger and its angular divergence becomes smaller when the Ag film thickness is increased from 30 to 100 nm. Aditionally, when the thickness of Ag film is increased to a complete mirror with Ag thickness of 200 nm, the BFP image (data not shown) remained same with similar emission intensity and angle as seen from the Tamm structure with 100 nm thick Ag layer. The strongest TPCE was found for the thicker Ag films. This phenomon can be understood as follows. The TPs are located mostly below the metal, in the top dilectric layer [41]. For low Ag thickness this mode does not exist so there is no coupled emission normal to the plane. At 55 nm and larger Ag thickness the TPs exist and TPCE is observed normal to the surface (Figure 5d and e). The TPCE becomes brighter with thickner Ag (100 nm) because emission into the air side cannot occur and this loss mechanism is blocked. In contrast to SPs, that exist on the air side of the metal, the TPs are under the metal and do not depend on the air side of the Ag film.

In adition to TPCE, the guided mode-coupled emission (GMCE) also appears on the BFP images. The GMCE is seen to depend on the orientation of the polarizer in front of the SCMOS camera. The location of the GMCE shows that its polarization is azimuthal, which means that the polarization direction of each point on the GMCE ring is along the tangential direction. As a result, the full ring is splitted into two parts due to the azimutally polarization of the GMCE as shown in Figure 5. In contrast to TPCE, the GMCE appears at all the five selective thickness of the Ag film. This is because the GMs are confined optical modes inside the 1DPC, so its apperances will not be influcenced greatly by the Ag films. Comparision of the five BFP images reveals an interesting phenomenon, the intensity ratio between the TPCE and GMCE on the same BFP image is enhanced with thickness of the Ag film. From the viewpoint of optical coupling, this phenomeon can be attributed to two factors. First, the TPs only exist for thicker Ag film. A second posible cause is that coupling of NB to the TPs is faster which takes energy away from the more slowly coupled GMs mode. At present, we cannot distinguish the two factors, but the experimental results shown

here clearly demonstrate that the TPCE become dominant with the increase of Ag film thickness. This issue may be resolved by time-resolved measurements of the TP and GM mode-coupled emission.

Based on the numerical simulations (blue strips on bottom of Figure 2a), SPs can be excited on the Tamm structures with thin Ag films, which will induce the SPCE. When the Ag film is 10 nm thick, no SPs are present and therefore no SPCE. When the Ag film is 20 nm and 30 nm, the SPs appear, but we did not observe corresponding bright and split SPCE rings. On the contrary, a pair of dark arcs appears on Figure 5(b) and (c). If the polarizer before the sCMOS is removed, a dark ring will appear (the corresponding BFP images not shown here). From the diameter of dark ring or arcs and known N.A. of the objective, the angle of this dip can be derived as about 42°, which is also larger than the TIRA. The reason for the dark rings or arcs can be explained as follows. In our experiment, the NB molecues are below the Ag films, while the SPs field is localized on the upper surface of Ag films. Some of the energy of the excited NB molecues can penetrate the Ag films will convert into the SPs, then the SPs can radiate back into the glass substrates. Due to the two penetrations across the Ag film, the SPCE will be greatly weakened, which means the SPCE will not be very bright. On the other hand, considering the white dashed-line box on Figure 2(a), there is a gap between the SPs and CMs. The reflectivity at this gap is as high as 0.97. The angle of this gap is around 41.8° which is consitent with the angular position of the dark dips on Figure 5 (b) and (c). As we know, the dip on the reflection curves, such as SPR dips, will display as bright SPCE rings on the fluorescence BFP image, similarly, the position with high reflectivty on the reflection curve (or reflected BFP image) will display dark on the fluorescence BFP image [49,55]. So the dark arcs on Figure 5 (b) and (c) can be attributed to modes gap on Figure 2 (a).

The fluorescence BFP image (Figure 5f) of the control Ag mirror shows a nearly uniform intensity distribution in the entire BFP image, which represents the random emission of the fluorescence or no directional emission from the control sample. This result shows the 1DPC under the Ag film is essential for the directional emission. Comparison of the six BFP images verifies that the combination of thick Ag film with the 1DPC can beam and enhance the fluorescence emission normal to the substrate at the resonant wavelength. The reason for the effect of the metal film on TPCE can be understood as following: TPs have in-plane wavevectors less than the wavevectors of light in vacuum, which allows for both direct optical excitation and free-space radiation. The TPCE not only radiates through the glass substrate, but also into the free space through the Ag films [41]. In this case, the TPCE should penetrate the Ag films. If the Ag films are thick enough (corresponding to high reflectivity), the TPCE cannot radiate into the upper space. As a result, the TPCE collected by the epi-illumination microscope (Figure 4 a) is enhanced.

4. Conclusions and outlook

In conclusion, the effects of metal films on TPCE have been investigated numerically and experimentally. The image plots of calculated reflectivity clearly demonstrates the dependence of TPs, SPs, and GMs on the top Ag films. At fixed incident angle or collection angle (for example near zero angle, resonant angle of the TPs), the measured reflection and

fluorescence emission spectra reveal different response of the Tamm samples to the wavelength at different thickness of the Ag films. At fixed wavelength (resonant wavelength of the TPs), BFP images of the fluorescence from the excited NB molecules coupling with Tamm strcutures presents emission intensity distributions which depend on the thickness of the Ag films. All of the experimental results are consistent with the numerical simulations. Our work indicates that the intensity of the TPCE will be enhanced, the angular divergence will be decreased when proper thickness of the Ag film is used. The TPCE will also be dominant over the SPCE and GMCE from the same Tamm structures. An understanding of the effect of metal film thickness on probes coupling with different modes is needed to design structures which are more suitable applications in sensing and diagnostics. The planar surface of the Tamm substrate and the high intensity near-normal fluorescence emission can be very useful for the high throughput fluorescence sensing or detection, and also high efficient light emitting devices. At the current stage, the fluorescent molecules are placed below the metal film, which are not very favorable for applications in fluorescence imaging. But this configuration may be useful in LEDs where the active mediums are always inside the structures. And also, if the extended metal films were replaced with structured or porous films, the fluorescence molecules may be placed on the top side of the Tamm samples.

Acknowledgements

The authors with USTC acknowledge the financial support by the National Key Basic Research Program of China under grant nos. 2013CBA01703, 2012CB922003, 2012CB921900. National Natural Science Foundation of China under grant nos. 61427818, 11374286, 61036005. This work was also supported by NIH Grants RO1HG002655, RO1EB006521 and GM017986.

References

1. Lakowicz, JR. Principles of fluorescence spectroscopy. third edition. Springer; 2006.
2. Wedge S, Wasey JAE, Barnes WL, Sage I. Appl. Phys. Lett. 2004; 85:182–184.
3. Lakowicz JR. Anal. Biochem. 2004; 324:153. [PubMed: 14690679]
4. Lakowicz JR. Anal. Biochem. 2005; 337:171. [PubMed: 15691498]
5. Yi MF, Zhang DG, Wen XL, Fu Q, Wang P, Lu YH, Ming H. Plasmonics. 2011; 6:213.
6. Fu Y, Zhang J, Lakowicz JR. J. Am. Chem. Soc. 2010; 132:5540. [PubMed: 20364827]
7. Zayats AV, Smolyaninov II. J. Opt. A: Pure Appl. Opt. 2003; 5:S16–S50.
8. Hutter E, Fendler JH. Advanced materials. 2004; 16:1685–1706.
9. Lakowicz JR, Shen YB, D'Auria S, Malicka J, Fang JY, Gryczynski Z, Gryczynski I. Analytical Biochemistry. 2002; 301:261–277. [PubMed: 11814297]
10. Zhang DG, Yuan XC, Bouhelier A. Appl. Opt. 2010; 49(5):875. [PubMed: 20154755]
11. Lakowicz JR, Malicka J, Gryczynski I, Gryczynski Z. Biochemical and Biophysical Research Communications. 2003; 307(3):435. [PubMed: 12893239]
12. Raether, H. Surface Plasmons on Smooth and Rough Surfaces and Gratings. Berlin: Springer; 1988.
13. Shalaev, VM.; Kawata, S., editors. Nanophotonics with Surface Plasmons. New York: Elsevier Press; 2007. p. 321
14. Ballarini M, Frascella F, Michelotti F, Digregorio G, Rivolo P, Paeder V, Musi V, Giorgis F, Descrovi E. Appl. Phys. Lett. 2011; 99:043302.
15. Ballarini M, Frascella F, Enrico E, Mandracci P, De Leo N, Michelotti F, Giorgis F, Descrovi E. Appl Phys Lett. 2012; 100:063305.
16. Angelini A, Enrico E, De Leo N, Munzert P, Boarino L, Michelotti F, Giorgis F, Descrovi E. New Journal of Physics. 2013; 15:073002.

17. Badugu R, Nowaczyk K, Descrovi E, Lakowicz JR. Analytical Biochemistry. 2013; 442:83–96. [PubMed: 23896462]
18. Michelotti F, Sinibaldi A, Munzert P, Danz N, Descrovi E. Opt. Letts. 2013; 38:616–618. [PubMed: 23455242]
19. Ballarini M, Frascella F, De Leo N, Ricciardi S, Rivolo P, Mandracci P, Enrico E, Giorgis F, Michelotti F, Descrovi E. Opt. Exp. 2012; 20:6703–6711.
20. Angelini A, Barakat E, Munzert P, Boarino L, De Leo N, Enrico E, Giorgis F, Herzig HP, Pirri CF, Descrovi E. Scientific Reports. 2014; 4:5428. [PubMed: 24962615]
21. Sinibaldi A, Fieramosca A, Rizzo R, Anopchenko A, Danz N, Munzert P, Magistris C, Barolo C, Michelotti F. Opt. Lett. 2014; 39:2947. [PubMed: 24978244]
22. Liscidini M, Galli M, Shi M, Decarro G, Patrini M, Bajoni D, Sipe JE. Opt. Lett. 2009; 34:2318. [PubMed: 19649083]
23. Aouani H, Mahboub O, Bonod N, Devaux E, Popov E, Rigneault H, Ebbesen TW, Wenger J. Nano Letters. 2011; 11:637. [PubMed: 21247202]
24. Aouani H, Mahboub O, Devaux E, Rigneault H, Ebbesen TW, Wenger J. Nano. Lett. 2011; 11:2400. [PubMed: 21591739]
25. Dregely D, Taubert R, Dorfmüller J, Vogelgesang R, Kern K, Giessen H. Nature Comm. 2011; 2:267:1–7.
26. Curto AG, Volpe G, Taminiau TH, Kreuzer MP, Quidant R, van Hulst NF. Science. 2010; 329:930. [PubMed: 20724630]
27. Belacel C, Habert B, Bigourdan F, Marquier F, Hugonin J-P, Michaelis de Vasconcellos S, Lafosse X, Coolen L, Schwob C, Javaux C, Dubertret B, Greffet J-J, Senellart P, Maitre A. Nano letters. 2013; 13:1516–1521. [PubMed: 23461679]
28. Rui GH, Abeysinghe DC, Nelson RL, Zhan QW. Scientific Reports. 2013; 3:2237. [PubMed: 23868718]
29. Rui GH, Chen WB, Abeysinghe DC, Nelson RL, Zhan QW. Opt. Exp. 2012; 20:19297.
30. Kaliteevski M, Iorsh I, Brand S, Abram RA, Chamberlain JM, Kavokin AV, Shelykh IA. Phys. Rev. B. 2007; 76:165415.
31. Gazzano O, Michaelis de Vasconcellos S, Gauthron K, Symonds C, Bloch J, Voisin P, Bellessa J, Lemaître A, Senellart P. Phys. Rev. Lett. 2011; 107:247402. [PubMed: 22243024]
32. Sasin ME, Seisyan RP, Kalitteevski MA, Brand S, Abram RA, Chamberlain JM, Egorov AYu, Vasilev AP, Mikhrin VS, Kavokin AV. Appl. Phys. Lett. 2008; 92:251112.
33. Symonds C, Lheureux G, Hugonin JP, Greffet JJ, Laverdant J, Brucoli G, Lemaitre A, Senellart P, Bellessa J. Nano Lett. 2013; 13:3179. [PubMed: 23777399]
34. Afinogenov BI, Besso nov VO, Nikulin AA, Fedyanin AA. Appl. Phys. Lett. 2013; 103:061112.
35. Das, Ritwick; Srivastava, Triranjita; Jha, Rajan. Opt. Lett. 2014; 39:896–898. [PubMed: 24562235]
36. Lee, Kwang Jin; Wu, JW.; Kim, Kihong. Opt. Exp. 2013; 21:28817–28823.
37. Das, Ritwick; Pandey, Awanish; Srivastava, Triranjita; Jha, J, Rajan. Light wave Technol. 2014; 32:1221–1227.
38. Auguié, Baptiste; Fuertes, María Cecilia; Angelomé, Paula C.; Abdala, Nicolás López; Soler Illia, Galo JAA.; Fainstein, Alejandro. ACS Photonics. 2014; 1(9):775–780.
39. Kaliteevski M, Brand S, Abram RA, Iorsh I, Kavokin AV, Shelykh IA. Appl. Phys. Lett. 2009; 95:251108.
40. Gazzano O, Michaelis de Vasconcellos S, Gauthron K, Symonds C, Voisin P, Bellessa J, Lemaître A, Senellart P. Appl. Phys. Lett. 2012; 100:232111.
41. Badugu R, Descrovi E, Lakowicz JR. Anal. Biochem. 2014; 445:1–13. [PubMed: 24135654]
42. Chen YK, Zhang DG, Qiu D, Zhu LF, Yu SS, Yao PJ, Wang P, Ming H, Badugu R, Lakowicz JR. Laser & Photonics Reviews. in press.
43. Rivolo P, Michelotti F, Frascell F, Digregorio G, Mandracci P, Dominici L, Giorgis F, Descrovi E. Sensors and Actuators B: Chemical. 2012; 161:1046.

44. Frascella F, Ricciardi S, Rivolo P, Moi V, Giorgis F, Descrovi E, Michelotti F, Munzert P, Danz N, Napione L, Alvaro M, Bussolino F. Sensors. 2013; 13(2):2011–2022. [PubMed: 23385414]
45. Farmer A, Friedli AC, Wright SM, Robertson WM. Sensors and Actuators B: Chemical. 2012; 173:79–84.
46. Konopsky VN, Alieva EV. Biosensors and Bioelectronics. 2010; 25:1212–1216. [PubMed: 19853435]
47. Toma K, Descrovi E, Toma M, Ballarini M, Mandracci P, Giorgis F, Mateescu A, Jonas U, Knoll W, Dostálek J. Biosensors and Bioelectronics. 2013; 43:108–114. [PubMed: 23291217]
48. For nasari L, Floris F, Patrini M, Canazza G, Guizzetti G, Comoretto D, Marabelli F. Appl. Phys. Lett. 2014; 105:053303.
49. Lakowicz JR, Shen YB, D'Auria S, Malicka J, Fang JY, Gryczynski Z, Gryczynski I. Analytical Biochemistry. 2002; 301:261–277. [PubMed: 11814297]
50. Zhang DG, Badugu R, Chen YK, Yu SS, Yao PJ, Wang P, Ming H, Lakowicz JR. Nanotechnology. 2014; 25:145202. [PubMed: 24621990]
51. Joannopoulos, JD.; Johnson, SG.; Winn, JN.; Meade, RD. Photonic crystals, molding the flow of light. second edition. Princeton university press; 2008.
52. Zhang DG, Fu Q, Yi MF, Wang XX, Chen YK, Wang P, Lu YH, Yao PJ, Ming H. Plasmonics. 2012; 7(2):309–312.
53. Hohenau A, Krenn JR, Drezet A, Mollet O, Huant S, Genet C, Stein B, Ebbesen TW. Opt. Exp. 2011; 19:25749.
54. Frisbie SP, Chesnutt C, Holtz ME, Krishnan A, Grave de Peralta L, Bernussi AA. IEEE Photonics Journal. 2009; 1:153–162.
55. Frisbie SP, Chesnutt C, Ajimo J, Bernussi AA, Grave de Peralta L. Opt. Comm. 2010; 283:5255.
56. Zhang DG, Yuan X-C, Yuan GH, Wang P, Ming H. J. Opt. 2010; 12:035002.

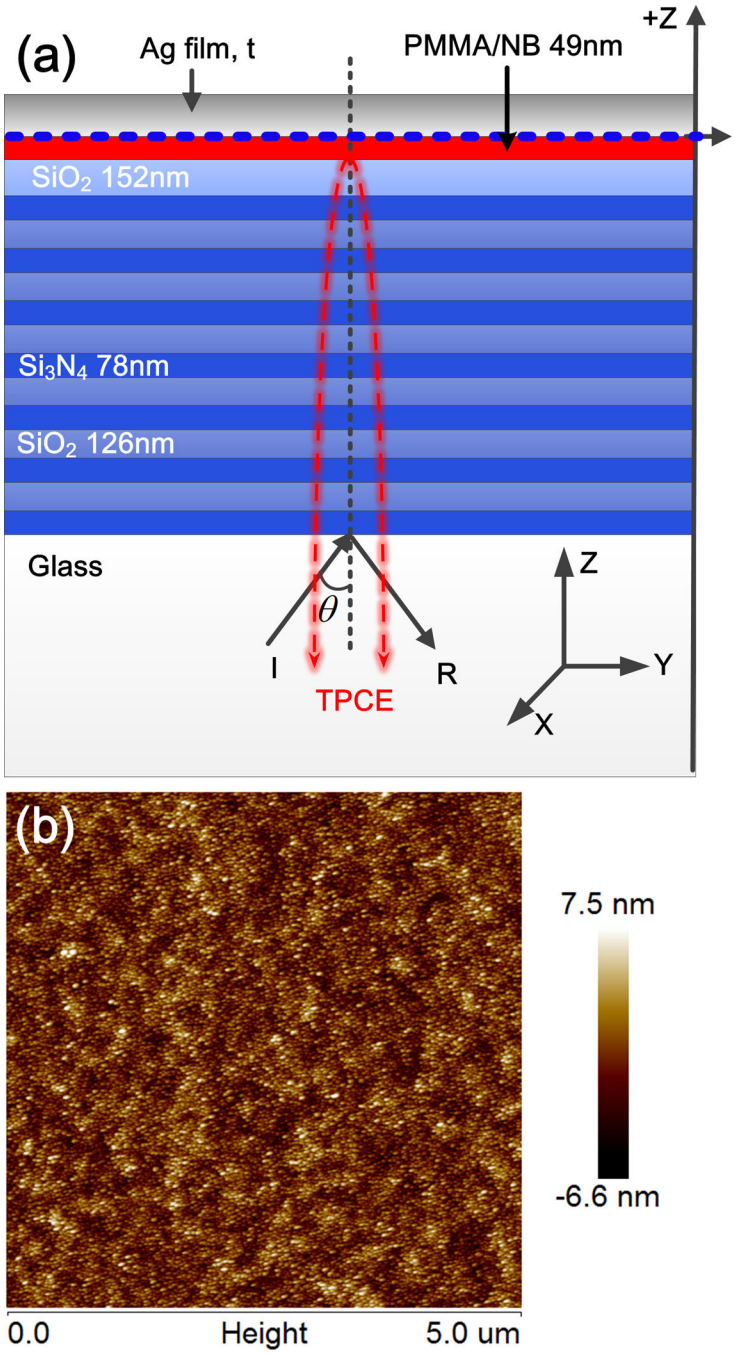

Figure 1.

(a) Schematic of the Tamm structure and layer dimensions. The thickness (t) of the top Ag film is varied from 0 to 200 nm. The Ag film is evapoarated on a one-dimentional photonic crystal (1DPC) which was previously coated with PMMA layer containing Nile Blue (NB) molecules. The thickness of each dieleteric layer of the 1DPC (SiO_2 and Si_3N_4) is shown in the schetmatic. (b), AFM image of the Ag film (with 10 nm thickness) on the 1DPC.

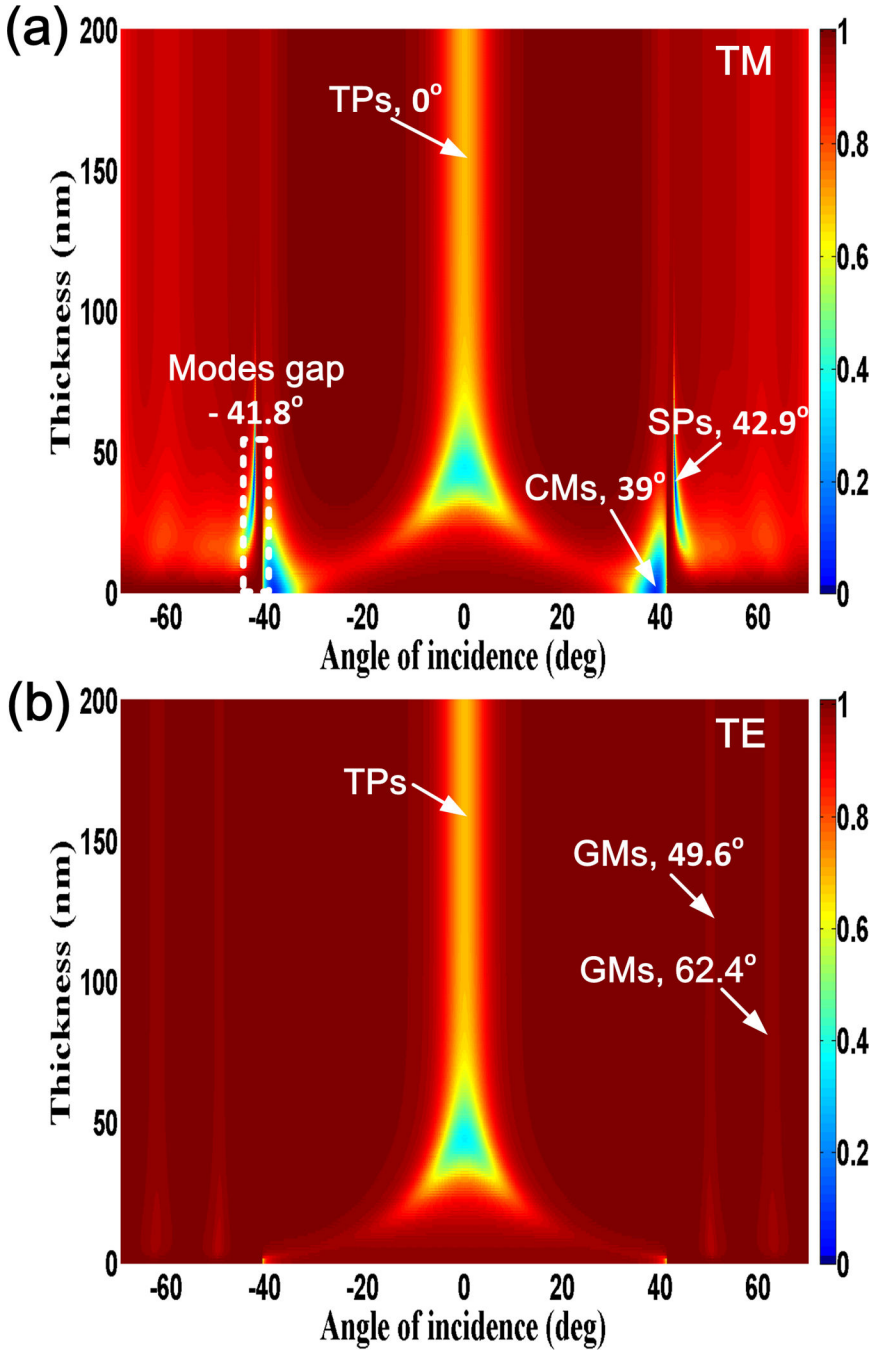

Figure 2.

Effect of Ag film thickness on the calculated angle-dependent reflectivity of the Tamm structure. The incident light wavelength is 680 nm with TM (a), and TE polarization (b).

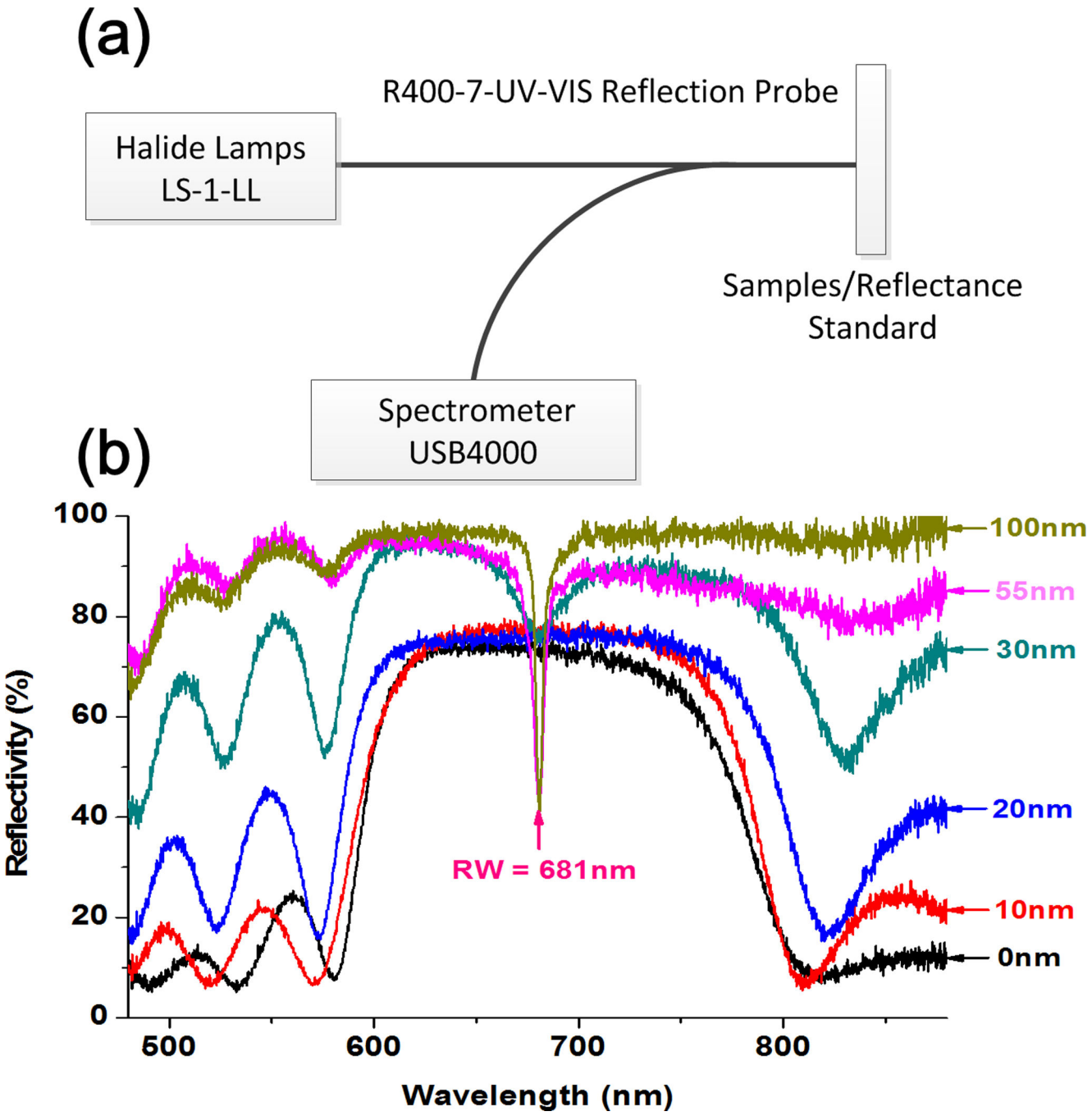

Figure 3.

(a) Schematic of the experimental set-up used to measure the reflectivity spectra of the Tamm structure at normal to the surface. (b) Measued reflectance spectra of the Tamm structures. The thicknesses of top silver layers are 0, 10, 20, 30, 55, and 100 nm.

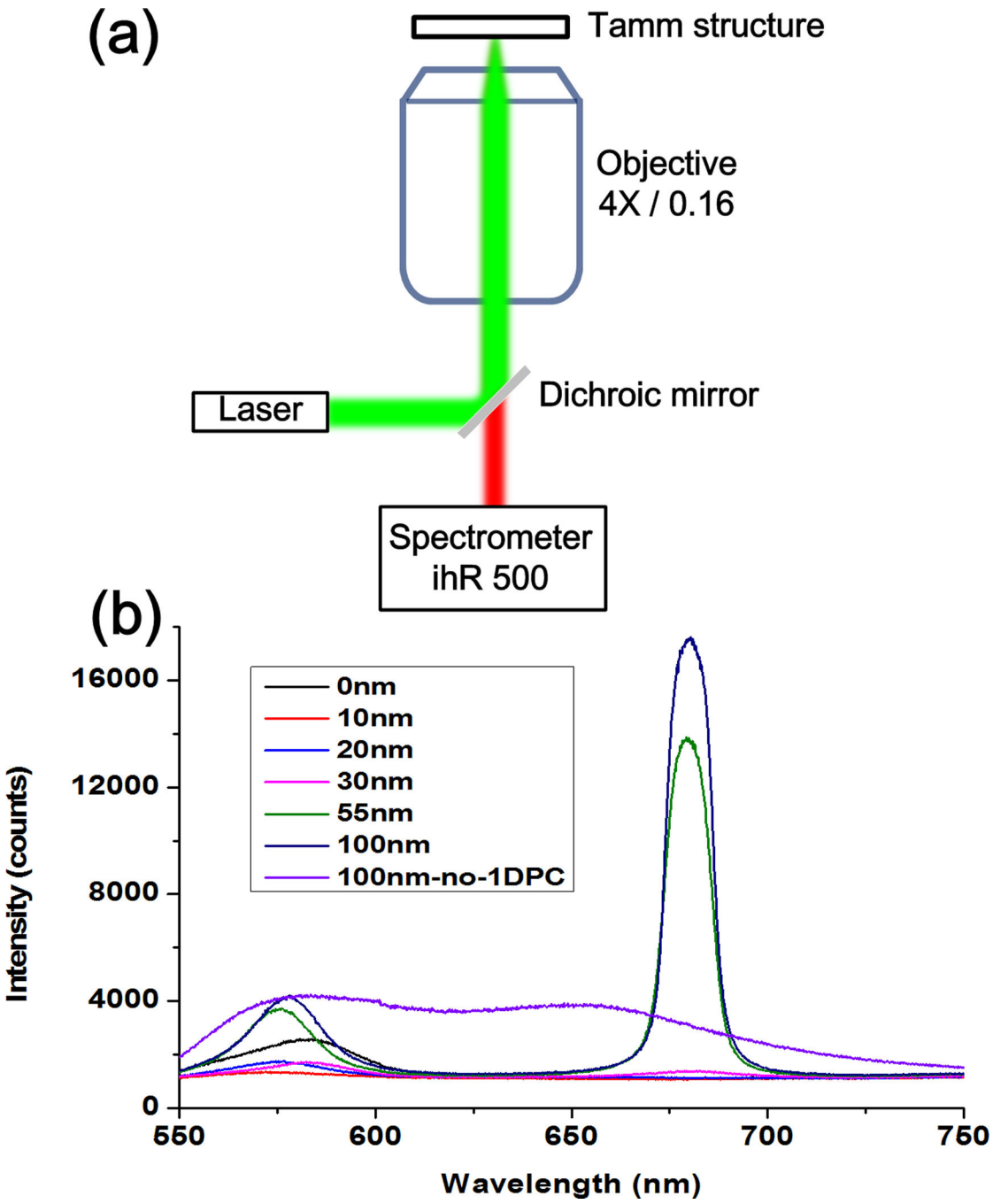

Figure 4.

(a) Schematic of the experimental set-up used to measure the TPCE spectra from the Tamm structures shown in Figure 1. An objective with low N.A of 0.16 is used to colleced the fluorescence emission normal to the surface of the Tamm substrates. Panel (b) shows the measured NB fluorecence spectra from the Tamm structures with varied top Ag layers thicknesses (0, 10, 20, 30, 55, and 100 nm). The fluorescence spectrum of a control sample without the 1DPC (Glass- 49 nm thick NB/PMMA- 100 nm thick Ag film) is also measured (100 nm-no-1DPC), which shows broad emission band.

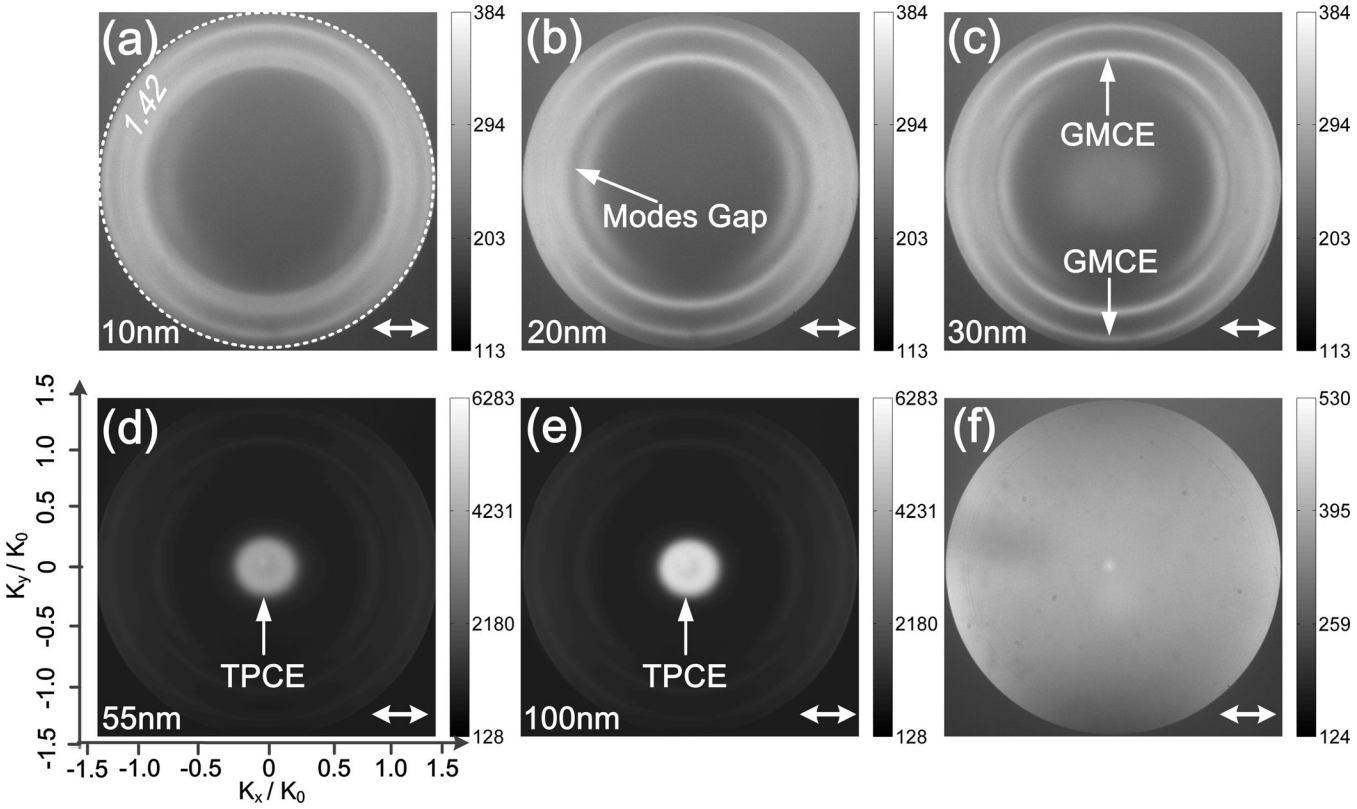

Figure 5.

BFP images of the NB fluorescence emission from the Tamm structures. The thicknesses of the top Ag layers are 10 (a), 20 (b), 30 (c), 55 (d), and 100 nm (e). The fluorescence BFP image of a control sample without the 1DPC (Glass- 49nm thick NB/PMMA- 100nm thick Ag film) is also measured (f). A band pass filter with center wavelength of 680 nm and a linear polarizer are used before the sCMOS camera (Andor). The double-headed arrows represent the direction of the polarizer. The white dashed circle on panel (a) represents the N.A (1.42) of the objective used in fluorescence imaging at BFP. The emitting angle (θ) of the coupled emission can be derived with the $\theta = asin((K_{x,y} / K_0)1.42 / 1.518)$, where $K_{x,y}$ is the wavenumber of the coupled fluorescence and K_0 is the wavenumber of light in vaccum.